applied sciences

MDPI

Article

Diagnosing Cracks in the Injector Nozzles of Marine Internal Combustion Engines during Operation Using Vibration Symptoms

Jan Monieta

Maritime University of Szczecin, Wały Chrobrego 1-2, 70-500 Szczecin, Poland; j.monieta@pm.szczecin.pl; Tel.: +48-91-48-09-415

Abstract: In the operation of internal combustion engines, despite technical state monitoring, some cracks that develop in metal components go undetected, leading to secondary, critical, or degradation damage. The diagnostic systems used in floating objects mainly use quasi-static thermodynamic signals, which alert operators too late about emerging damage. Although various methods have been developed to detect cracks in internal combustion engine components, the effectiveness and implementation of the proposed methods are not satisfactory. Therefore, this article presents the use of selected vibration and in-cylinder pressure signals to diagnose the development of damage in some components of marine diesel engines. The investigations were conducted under the natural conditions of the operation of sea-going vessels during port-handling operations. During these investigations, it was possible to observe clear changes in the values of diagnostic symptoms, which corresponded to the development of damage. The developing damage detected in the study involved cracks in injector nozzles manufactured from alloy steel. Despite advances in design, materials, and manufacturing technology, injector nozzle cracks still occur. The diagnostic symptoms used to detect damage development were the amplitude and spectral and wavelet measurements of vibration acceleration signals. This work aimed to search for crack-oriented methods of signal analysis, for example, computer visualization and the recording of diagnostic parameters in various domains. Decimation, windowed, time, amplitude, and time-frequency domain analyses; wavelet statistics; color analysis; and machine learning were used for classification using artificial neural networks. Experimental investigations showed the possibility of diagnosing the development processes of damage to marine diesel engines. The advanced signal processing methods used made it possible to obtain many signal measurements, from which the most useful diagnostic symptoms were selected. The new symptoms found with decimation, time-domain windowed analysis, and Haar wavelet statistics were more useful than the existing ones.

Keywords: marine engines; residual processes; diagnostics; vibration signals; detection of damage development

Citation: Monieta, J. Diagnosing Cracks in the Injector Nozzles of Marine Internal Combustion Engines during Operation Using Vibration Symptoms. *Appl. Sci.* **2023**, *13*, 9599. https://doi.org/10.3390/app13179599

Academic Editors: Jong-Myon Kim, Cheol Hong Kim and Farzin Piltan

Received: 12 June 2023
Revised: 2 August 2023
Accepted: 5 August 2023
Published: 24 August 2023

1. Introduction

Vibroacoustic diagnostics include vibrations, noise, medium pulsation, and acoustic emissions [1,2]. Vibroacoustic signals are measured using sensors to process the primary physical quantities of objects:

- Element displacement;
- The velocity of elements;
- The acceleration of elements;
- The phase shift of harmonic portions;
- Pressure;
- Strength;
- Stress.

For the measurement of vibroacoustic signal generation, piezoelectric sensors, called accelerometers, are most often used, as they have a wide range of measurement frequen-

cies, high dynamics, and good linearity and are stable for long periods [3]. Degradation processes in power facilities affect the evolution of load distribution, which indicates the desirability of using frequency analyses of vibration signal systems and studying the impact of damage development on signal changes. According to some authors, there are better tools than classical spectral analyses, in which an assumption of mutual independence of components is made [4].

Intelligent systems have been constructed and used in this field, operating according to algorithms that include the detection and localization of damage [5]; the assessment of the degree of criticality of a state; changes in parameters as a result of a response to a change in a technical state; and forecasting the remaining existence time. Algorithms for the adaptive control of internal combustion engines with changing dynamic properties as well as changing properties and stochastic disturbances have also been used, during which process and disturbance model parameters are estimated in order to update the control algorithm. When assessing risk, it is possible to use analysis methods such as fault and event trees, considering the influence of wear processes and impacts on the environment. Measuring energy bandwidth changes in the spectral width ratio can be used to assess damage development [6].

Radkowski and Jasiński [7] proposed a method of predicting and analyzing the giga-cycle fatigue life of gear materials using a vibroacoustic signal. The authors carried out accelerated fatigue tests on a constructed stand operating in the natural frequency range of the samples. The vibroacoustic diagnostic methods enabled the detection of surface damage and damage in the core of the sample. Their research allows for an understanding of the nature of the increased fatigue life and to use of the parameters of vibroacoustic signals to predict fatigue life.

Miesovich et al. [8] indicated that changes in mild steel and high-strength steel samples cause changes in observed acoustic emission signals. Fatigue cracking shows different stages of development [8], namely substructural and microstructural changes, the microscopic formation of dominant cracks, the stable propagation of dominant cracks, and structural instability leading to the termination of the cracking. Although various methods have been developed to detect fatigue cracks [6,8], detecting crack initiation remains a real challenge in nondestructive testing. The main problem of the early microstructural stage of fatigue cracking is its stochastic nature. Radkowski found that higher-order central statistical moments reveal the most information when diagnosing damage using vibroacoustic signals [6].

Another study described a stress assessment methodology and a method of integrity loss detection for concrete beams using a technique based on vibroacoustic signal analysis [1]. The skeletal curve of nonlinearity changes obtained in the experiment, after the secondary processing of a time-frequency map, showed that the difference in the shape of the skeletal curve was correlated with the change in stresses in the structure. Qualitative changes in nonlinearity were used to detect the loss of cohesion in the examined systems. After the secondary processing of a time-frequency map, the nonlinearity changes obtained in the experiment skeletal curve were used to detect the examined system's cohesion loss. During the operation of internal combustion engines, some components gradually degrade, leading to damage that, at a particular instant, is invisible to the user. In the early stages of damage development, there are changes in the frequency structure of the signal. The sensor's location is important for measuring vibroacoustic signals because the signal carries many of the processes in the engine. Therefore, the choice of sensor location significantly impacts the quality of information in a given signal and the accuracy of diagnostic decisions [9,10].

For the case of the cracking of internal combustion engine components (i.e., shafts and nozzles), durability was defined as the number of cycles of stress changes, the number of repetitions of a specific load block, or the working (operation) time necessary for stable growth in cracking from an assumed initial dimension to a specified final extent [3,4,10].

In addition, cracks occurring in the mechanical elements of internal combustion engines cause vibration energy dissipation [3].

Czech et al. [11] used noninvasive methods of vibroacoustic phenomena to diagnose a combustion engine fault. The noninvasive methods were essential in planning studies based on vibration and acoustic signals. The authors applied discrete wavelet transforms and probabilistic neural networks for signal analysis. Moreover, in another study [12], Czech presented trials of using vibration signals generated with a four-cylinder car combustion engine to diagnose a fuel injector state.

One of the diagnostic methods of combustion engines is dilatometry, which deals with methods of measuring the thermal expansion of materials [13]. The authors investigated the dilatometric methods for damage diagnosis and engine damage formation. Research reveals that two cases of malfunction relate to needle-nozzle holder precision pairs of self-ignition engines. Different thermal expansions of these pairs cause changes in clearances and friction energy [14].

In another study, many injector nozzles used in self-ignition engines cracked [15]. The damaged nozzles were composed of 38CrMoAl steel and were nitride. The investigations revealed that the main damage modes are longitudinal and circumferential cracking on the external surface of the head region and the dent at the head tip. Metallurgical examinations showed that the present cracking failure of the nozzles is not related to the metallurgical defects and the strike on the heads by other objects.

In addition, Yu and Xu examined cracked injector nozzles composed of 18CrNi8 carburized steel [16]. Fractographic studies indicated that the origin of the crack was in an oil-filled groove within a thin wall, and a brittle intergranular fracture was the cause of the damage to the injector nozzles. Metallurgical studies performed with a spectroscope showed that brittle Al_2O_3 inclusions were present in crack areas, and the stress concentration around the inclusions promoted crack initiation.

Asi [17] conducted a damage examination of a self-ignition engine injector nozzle used in a truck. The nozzle was produced from 18CrNi8 case-hardening steel, and it cracked after about 400 h operation. Integrity assessment was performed on the injector nozzle via photo documentation, chemical analysis, microhardness measurement, metallographic investigation, and scanning electron microscopy. The research results showed that the damage occurred because of cavitation wear in the internal surface of the nozzle body, followed by fatigue cracking.

Galle et al. [18] studied injectors for bio-oil supply that suffered premature damage from 50 to 1500 h operation. They found plastic deformation, channel obstruction, micro-cracking, erosion, and cavitation damage. The authors concluded that the chemical and physical composition of the fuel caused damage to the injectors.

Changes in the technical state of the engine, which are caused by the early stages of wear and damage, are difficult to detect. Therefore, an essential issue in engine vibration tests is the appropriate interpretation of complex measurement signals through increasingly more perfect signal processing methods [19]. The main tasks in diagnosis include the separation of useful signals and the determination of the characteristic parameters of the processed signals sensitive to faults.

The imperfection of operational tests is the difference between the instant of occurrence of the unfitness and its finding. Due to the severe secondary failure, selecting the injection apparatus for diagnostics is expedient [9]. The advantage of the proposed method is that it detects damage before the failure and, based on the prediction model, determines the time remaining for a critical failure. The difference between the proposed work and others in the literature is the presentation of the application of selected advanced signal processing methods, including classification and machine learning in neural networks.

Namigtle-Jiménez et al. [20] used classical signal analysis to diagnose injector faults in the time and frequency domain. Korczewski [21] presented the study assumptions of the identification of slowly varying energy processes in high-cycle fatigue of structural materials of a diagnostic ship propulsion system. In addition, the author presented the

results of preliminary experimental tests conducted on a Schenck fatigue test machine using vibration acceleration measurements, acoustic emissions, and infrared radiation temperature. Miesovich et al. [8] indicated that changes in mild steel and high-strength steel samples cause changes in the observed acoustic emission signals.

Machine learning and classification have also been used to diagnose damage development in internal combustion engines. Tabaszewski and Szymanski [22] presented the use of a vibration signal to classify valve clearance using machine learning. Among other factors, the authors developed a classifier as a neural network and a *k*-nearest neighbor algorithm.

Instability, nonlinearities, significant noise, and unstable operating conditions characterize diesel engine vibration signals. Zhao et al. [23] proposed a method of improved wavelet packet frequency and convolutional neural network to diagnose valve train faults. They developed time-frequency distribution feature matrices with mean packet-Mel frequency cepstral coefficient and wavelet distribution frequency bands. The authors also used a hierarchical structure and vibration signal state neurons. The study's results validated the method's efficiency in the diagnosis of the valve clearance of self-ignition engines.

The largest portion, i.e., around 59%, of undesirable events in marine power plants are damage to the main and auxiliary engines. Removing such effects accounted for 34% of all costs incurred in the period under review [9,24].

Wang et al. [25] applied the Bayesian neural network model to a marine self-ignition engine's performance prognostics to monitor its state. The Bayesian logistic regression model quantifies the development damage process of the marine compression ignition engine. The authors showed that the proposed approach is superior to the other online technical state monitoring methods for prognostics.

Niu et al. [26] compared artificial neural networks (ANNs) and support vector machines (SVMs) in their study on predicting the response of marine diesel engines supported by a common rail direct injection system. The authors demonstrated that SVM was well suited for predicting engine response with limited, expensive experimental data.

Chybowski et al. [27] described the analysis and causes of the cracking of the nozzle body of marine self-ignition engines. In a cause-effect study, the authors applied the theory of inventive problem solving (TRIZ) for various damage hypotheses. Modern marine diesel engines have a computerized control unit, which usually has self-diagnostic capability. However, marine systems have no prevailing standard, and obtaining condition information requires expensive equipment. Monitoring is often intermittent, and data must be periodically downloaded and analyzed [28].

A literature review reveals a lack of studies on the detection of developing cracks, especially in the nozzles of internal combustion engine injectors, during the operating phase. It was found that, although research has been performed on a wide range of methods, only a selection of studies are mostly focused on the cracking of injector nozzles of marine engines. Furthermore, the use of neural network classification for the detection of such damage has not been encountered in the literature. An attempt to fill these gaps in the existing diagnostic studies of internal combustion engine components of assemblies is undertaken in this article.

This research presents the problems related to the identification of parameters for the detection of the growth of fatigue cracks in an injector nozzle of a medium-speed marine diesel engine using signal analysis methods in the decimation, windowed, time, amplitude, frequency, time-frequency domain, and wavelet transforms. The developing damage led to a critical failure that ended the operation of the internal combustion engine, which was detected in many domains of signal analysis.

This article offers a methodology for planning an experiment to select the parameters for the real-time monitoring of fatigue crack initiation and propagation, which is very important for the safe operation of transportation means. This allowed us to obtain many diagnostic symptoms of vibration signals in various domains, from which the most useful and new ones were selected against the background of existing ones.

This contribution consists of finding the most useful symptoms and determining the lower and upper limits that separate the state of a developing crack in an injector nozzle.

2. Materials and Methods

2.1. Research Objects

The research objects were based on a marine internal combustion engine type 6AL20/24D used to drive generators on sea ships. The AL20/24 engine is an in-line, nonreversible, water-cooled, and four-stroke self-ignition engine with direct fuel injection, supercharged using a turbocharger, and charge air cooling. The basic engine specifications are presented in Table 1.

Table 1. The specifications of the 6AL20/24D engine.

Size	Value and Unit
Engine type	6AL20/24D
Type of construction	in-line, 6 cylinders
Direction of rotation	right
Firing order	1–4–2–6–3–5
Rated speed	750 rpm
Mean piston speed	6 m/s
Cylinder bore	200 mm
Piston stroke	240 mm
Troke volume	7540 cm^3
Rated power per cylinder	70 kW
Compression ratio	1:12.7
Medium effective pressure	1.48 MPa
Injector opening pressure	24.5 (40) MPa
Maximum combustion pressure	12.95 MPa

The injectors of the tested engines were modernized during production, in which the opening pressure was increased from 25 to 40 MPa. The nozzles had different designs of spray holes and were manufactured by other producers [29]. The injector nozzles had informative markings. For example, $159^\circ \times 07 \times 0.26R$ meant that the holes were at an angle of 159° in the number of 7 with a spray hole diameter of 0.26 mm, and the holes were EDM-rounded. Nozzle bodies of the rounded spray holes from the inlet side were marked with the letter *R*. Rounding the spray holes from the inside of the body was aimed to change the fuel injection characteristics and stable operation of the nozzle during operation [29].

The concerning damage to the nozzles was found to be the breaking of the nose or a larger fragment of the nozzle body of combustion engine injectors due to crack propagation. The surface of the nozzle body is nitrided and, therefore, hard. The injector nozzles are subjected to various mechanical forces during transport, assembly, and disassembly as well as cyclic mechanical, thermal, and hydraulic loads. The appearance of microcracks in the injector nozzles causes them to propagate during operation and eventually lead to the breaking of a fragment. If a piece of the injector breaks off, serious secondary damage can occur after another movement with the exhaust fumes.

An example of secondary damage to the turbocharger rotor caused by a broken nozzle head is shown in Figure 1. In another such event, the piston and cylinder liner, apart from the turbocharger, were damaged. Finally, in a very severe event, the ship caught fire due to damage to the fuel filter, and the crew had to be evacuated.

The hull was subjected to heat treatment, stress relief annealing, and nitriding with a thickness of 0.6 mm and hardness of 1000–1100 HV after nitriding, grinding, and lapping the guiding parts.

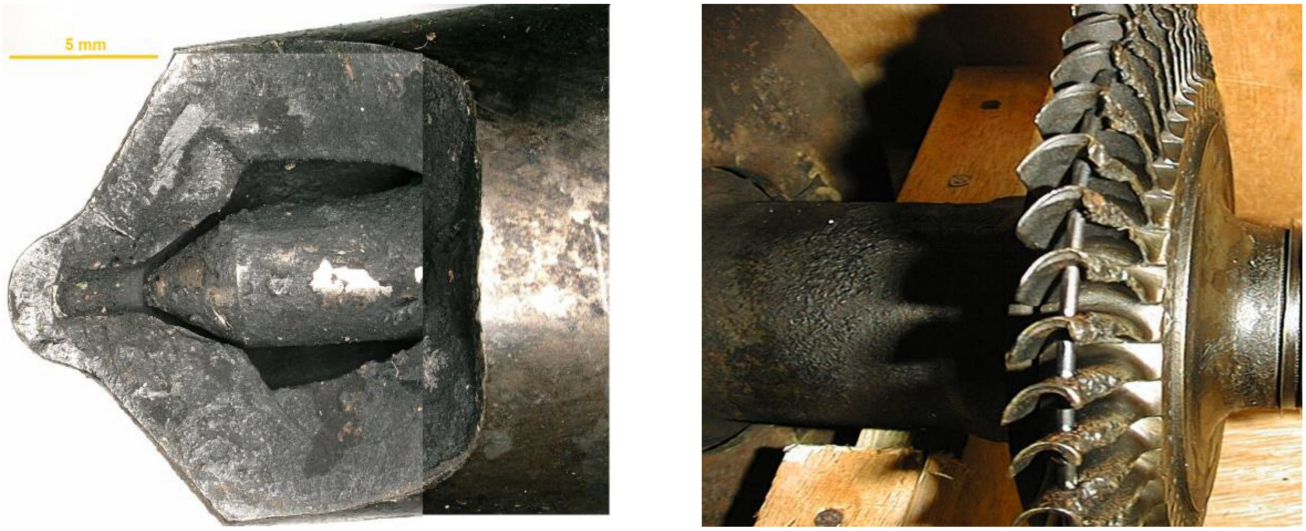

Figure 1. View of the nozzle of the injector 159 × 9 × 023*R* with a piece broken off (**a**) and the turbine rotor damaged by fragments of the nozzle (**b**).

2.2. Research Method

The choice of sensor location significantly impacts the quality of the information in a given signal and the accuracy of diagnostic decisions [3,9,10].

Based on preliminary studies [3,9,10,30,31], the following measurement points were selected: engine component locations with the highest unreliability and the area with the highest vibration signal generation level. The vibration signal, recorded anywhere on the engine body, is a weighted sum of the responses to all elementary events. The weights are convolutions with impulse functions of the transition from the place of generation to the reception of the diagnostic signal. The received vibration acceleration signals were in three channels, and each channel took a component of the vibration signal in one of three directions: parallel, horizontally perpendicular, and vertically perpendicular to the axis of the injection pipe.

One of the methods of obtaining diagnostic information is the measurement of vibrations generated by a piston combustion engine. Therefore, an attempt was made to diagnose marine diesel engines using vibration signals in various directions and simultaneously measuring the pressure signals in the combustion chamber and vibrations [31]. The architecture of a computer measurement system that provides support for sensors in terms of the power supply, signal loading, the preprocessing of the measured analog signals, synchronous or asynchronous analog-to-digital processing, analysis of selected signals and their archiving, and the transfer of signals to the database and knowledge base was presented in previous studies [9,32]. The measurement system consisted of vibration accelerometers and preamplifiers from Brüel and Kjaer, a photo-optical crankshaft position sensor, a terminal block, and a portable computer (Figure 2). The accelerometers were attached to the injection pipe with a portable bracket. As a result, the design of the injection subsystem was not affected, which is a requirement for classification societies.

During diagnostic tests, passive and passive-active diagnostic experiments were conducted. The tests were carried out for all cylinders with the same repetitive loads, resulting from the power consumption of the receivers under the natural conditions of a seagoing vessel. Rotational speeds were nearly nominal at the same level as the internal combustion engine that drove the generators. The measurements of vibration accelerations were performed at experimentally determined points of the injection subsystem for various types of diesel engines in addition to the type 6AL20/24D presented in this article in a sea vessel.

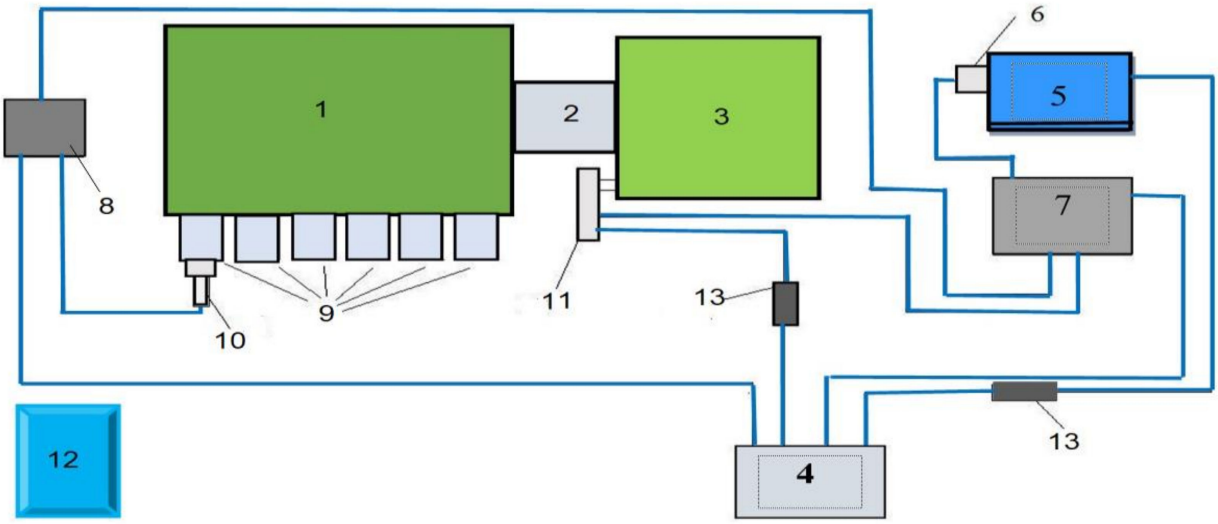

Figure 2. Schematic of the measurement system: 1—marine diesel engine, 2—shaft, 3—generator, 4—power strip, 5—laptop, 6—measurement card, 7—terminal block, 8—preamplifier, 9—injection pipe, 10—acceleration vibration sensor, 11—photo-optical crankshaft position sensor, 12—monitor for visualization of generator set loads, 13—power supply.

The following parameters were determined during the acquisition and analysis of diagnostic signals: analysis domain, frequency bands, the number of signal averaging, the use of filters, etc. The effect of the frequency band on the analysis results was examined, and the selected band for these tests ranged from 0 to 10 kHz for vibration acceleration signals and from 0 to 2.5 kHz for the in-cylinder pressure signals.

The DaqView computer program from IOtech was used for signal acquisition. DaqView is a configuration and measurement software that operates with measurement systems from various companies. The integrated data acquisition system consisted of a device archiving a large volume of data in the main memory, controlled with a portable computer, and recording and analyzing systems. This enabled the configuration of the devices and measurements. This software allows one to select these settings, observe the measurement results, and save them in real time. Using this program, selected signal analyses were performed in various domains, and the resulting data were transferred to other programs. The test data were recorded alongside the measured values of the reference conditions and converted to normal conditions according to the ISO 3046-1:2002 (E) standard.

The measurement signals were analyzed in the domain of time, decimation, windowed, frequency, time-frequency, amplitude, and wavelet transforms to find the most damage-oriented diagnostic symptoms. The limits were determined with a probability of 99.7% for the obtained mean values of the diagnostic parameters. These were the downward and upward deviations of the errors of the mean-squared arithmetic means from the mean values according to the following relationship:

$$a_{llv} = a_{aver} - 3\sigma_s \tag{1}$$

$$a_{ulv} = a_{aver} + 3\sigma_s \tag{2}$$

where a_{llv} is the lower limit value of the diagnostic parameter, a_{ulv} is the upper limit value of the diagnostic parameter, a_{aver} is the average value of the diagnostic parameter, and σ_s is the mean-squared error of the arithmetic means calculated from the following relation:

$$\sigma_s = \sqrt{\frac{1}{n(n-1)} \sum_{i=1}^{n} (a_i - a_{aver})^2} \tag{3}$$

where a_i is the *i-th* value of the diagnostic parameter, and n is the number of measurements.

The processed signals were analyzed in MS Excel, MATLAB, and Statistica computer software environments, where useful diagnostic symptoms were sought. The investigations were carried out during 247 h of operation before the occurrence of secondary failure.

The measured values of the diagnostic parameters for the six cylinders of the engine were analyzed using the classification learner application in MATLAB 2022a computer program, and classification was achieved using artificial neural networks in Statistica 13.3 environment. Data were divided into learning, testing, and validation and subjected to machine learning.

Injector nozzle fractures were investigated using geometric and flow measurements [33] and image analyses [34]. Images of the samples were obtained with a digital microscope (XRECx1000 type) at magnifications between 40× and 4000× and an optical microscope together with a Nikon Coolpix 4500 digital camera and a VHX-6000 digital microscope. The Nikon Coolpix 4500 camera was also used to record the images of the tested oils. The results correspond to significant fuel leakage from a damaged injector nozzle. Tests of diluted lubricating oil were performed at Werner Herrmann Castrol, Germany. The degradation tests of the fuels, engine oils, and deposits were also carried out using the methods described in [34].

3. Selected Research Results

3.1. Analysis of Signals in the Time Domain

The analysis involved the dynamics of the mechanical components of the injection subsystem, which include the nozzle and the injector spring (Figure 3). The equation of the dynamics of movement of the nozzle needle during fuel injection can be described as follows:

$$m_w \frac{d^2h}{d\tau^2} + A_g \frac{dh}{d\tau} + k_{sw}(h + h_{wo}) - p_w(A_{ip} - A_i) - p_s A_i = 0 \quad (4)$$

where A_g is the flow area through the firing pin seat, A_i is the cross-sectional area of the firing pin, A_{ip} is the cross-sectional area of the firing pin guide part, h is the instantaneous stroke (displacement) of the firing pin of the injector, h_{wo} is the initial tension of the injector spring, k_{sw} is the spring constant of the injector, m_w is the mass of the moving parts of the injector, p_w is the pressure in the chamber of the injector, p_s is the pressure in the sack of the injector nozzle, and τ is time.

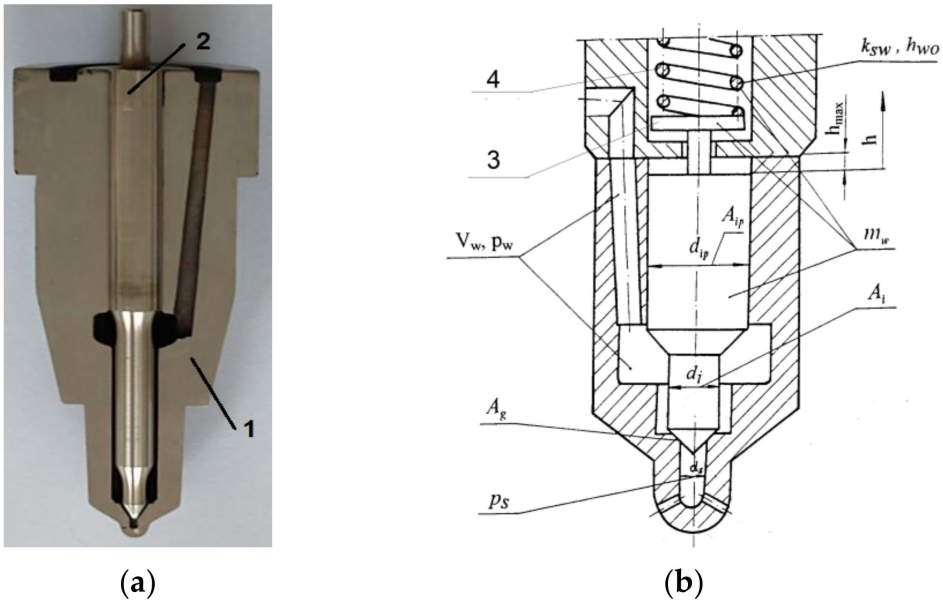

Figure 3. Cross-section of the injector nozzle including the needle (**a**) and diagram of the injector space (**b**): 1—injector nozzle body, 2—injector needle, 3—injector pin, 4—spring.

The first term in Equation (4), $a = dh^2/d\tau^2$, is the acceleration of the injector needle.

This equation describes the loads acting on the injector nozzle, which initiate and propagate the cracks. Simultaneously, the first term of Equation (4) relates to the mass of the needle, the vibration acceleration, and the amplitude of the vibration acceleration at a certain time $a = f(\tau)$.

Analyzing the diagnostic signals in the time domain allows one to obtain the time waveform of a single call and averaged signals [9]. Here, it is possible to determine the process waveform's beginning, end, and duration. Signals were recorded as time-domain waveforms using the time selection with an opening interval. However, due to numerous worldwide time-domain studies, in this work, more detailed analyses of diagnostic signals were not conducted in this area. By contrast, decimation and windowed analysis of time waveforms are considered innovative. Figure 4a shows the time waveforms for cylinder No. 1 in the suitability state and before damage in No. 5. Figure 4b shows the time waveforms of in-cylinder pressure No. 3 of auxiliary engine No. 2 and in cylinder No. 5 of auxiliary engine No. 3. Due to the abnormal pressure waveforms of the three cylinders of test engine No. 2, caused by the malfunctioning of the indicator valves, they were not measured in the other cylinders. There are also marine engines without indicator valves, for which measuring cylinder pressure waveforms is difficult [31].

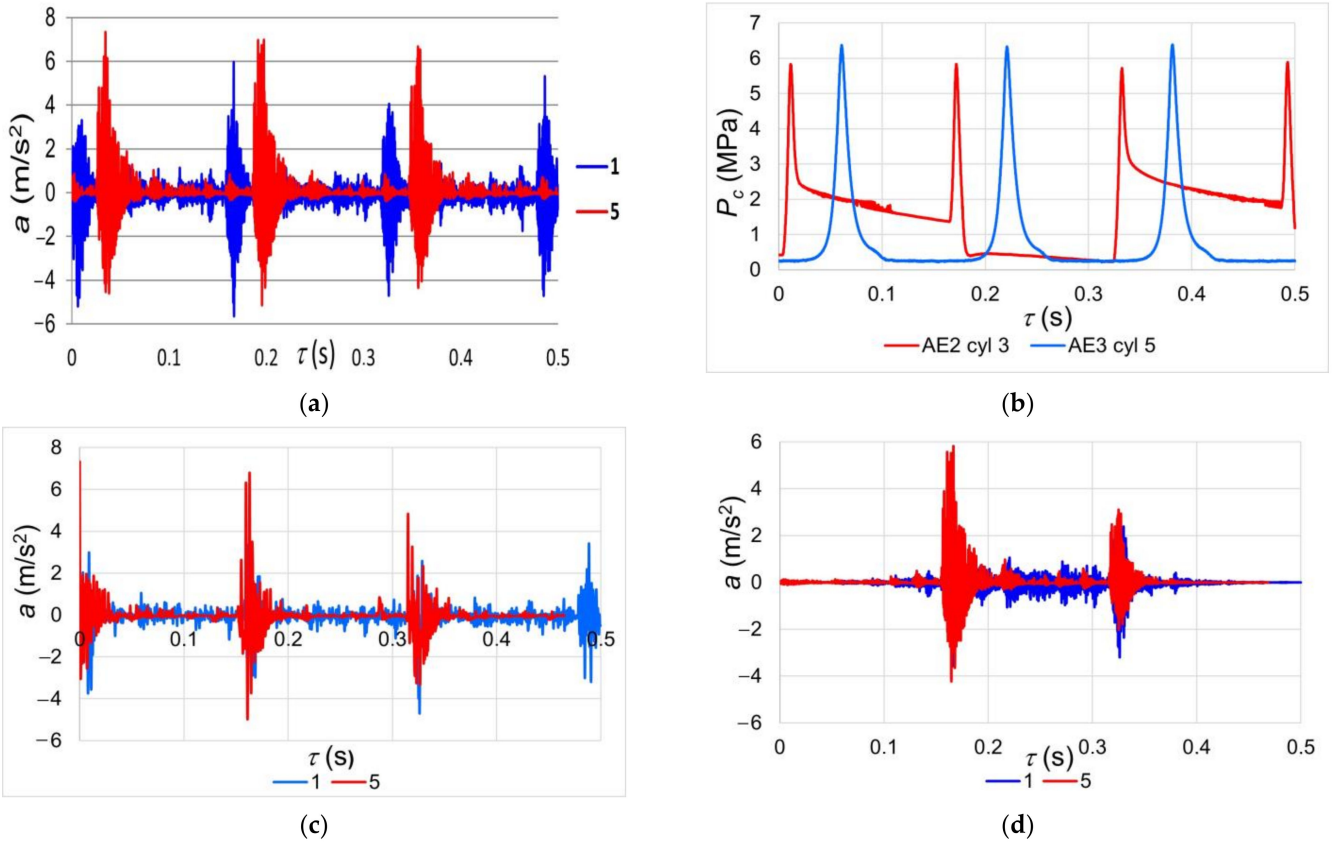

Figure 4. Time waveforms of vibration acceleration signal (**a**), in-cylinder pressure (**b**), decimation (**c**), and the result of windowed analysis (**d**) of the vibration acceleration signal *a* for cylinder No. 1 in an upstate and cylinder No. 5 with a working time of 247 h before damage detection.

Decimation transforms a discrete signal, which involves retaining every *Mth* sample and discarding the rest. Denoting the input and output signals as a_x and a_y, respectively, this decimation can be written as follows:

$$a_y(n) = a_x(Mn) \quad (5)$$

where M is the decimation factor. The signal after M-fold decimation contains M times fewer samples than before, which means it was sampled at M times lower frequency (Figure 4c). On the other hand, Figure 4d shows another sought-after innovative method of signal analysis: windowed time. The windowed analysis of a signal changes the shape of the waveform in the time domain; when this method was used, equal signal variation was possible for the suitability state and the developing crack.

The visualization of signals for the state of suitability before failure and the values of correlation and sensitivity coefficients showed significant differences between the analyses in these domains. The coefficient of correlation and sensitivity between the cylinders was calculated by determining the relationships between the state features and diagnostic parameters or by comparing the time waveforms and spectra for the reference cylinder and the other cylinders. Correlation and sensitivity coefficients for individual cylinders were found based on the relationships between diagnostic parameters and input values, such as the technical state or load of the internal combustion engine. The most useful symptoms are those whose correlation coefficient values between the state of suitability and developing damage were closest to 0.00 and reached the highest sensitivity coefficient values. Optimization was performed due to the selected criteria [9]. The most significant values of these coefficients were obtained for windowed time analysis and decimation, followed by Haar wavelet statistical measures.

In the study of damage development, comparisons were made between current and reference time waveforms, and the correlation coefficients between them were determined. It is only possible to effectively evaluate signals with the time-domain visualization of the raw signals, and various advanced signal processing like decimation is possible.

3.2. Analysis in the Domain of Amplitudes

The functional, dimensionless, and point estimates can be determined in this type of analysis. Most point estimates are determined for a (single) instantaneous signal or successive sequences of signals. Due to the random component in the observed vibroacoustic process, each measure is averaged over the corresponding dynamic time interval τ, with the segment T (Hann window) called the observation time.

In the amplitude domain, point estimates were determined for recorded instantaneous time waveforms of vibration acceleration signals: root-mean-square *rms*, average *aver*, and peak-to-peak (*p-p*) values. The formulas for these global point measures for $0 \leq \tau \leq T$ are as follows:

– Root-mean-square value:

$$\widetilde{a}(\theta) = \left[\frac{1}{T}\int_0^T a^2(\tau,\theta)d\tau\right]^{\frac{1}{2}} = a_{rms}(\theta) \tag{6}$$

– Average value:

$$\bar{a}(\theta) = \frac{1}{T}\int_0^T |a(\tau,\theta)|d\tau = a_{aver}(\theta) \tag{7}$$

– Peak-to-peak value:

$$a_{p-p}(\theta) = \{max[+a(t,\theta)] - max[-a(t,\theta)]\} \tag{8}$$

where τ is the dynamic time, T is the observation time, and θ is the object existence time.

Examples of the signal analysis results in the amplitude domain (peak-to-peak values, root-mean-square values, and average values) are shown in Figure 5a. Figure 5b displays the *rms* values of the vibration acceleration signals measured in the injection subsystem around the estimated limit values. As shown in Figure 5b, for the developing damage, the frequency of the component amplitudes shifted toward lower frequencies, which affected the value of the correlation coefficient k = 0.0974 between the spectra for cylinders No. 1

and No. 5. Cylinder No. 5 exceeded an upper limit value just before failure, but No. 4 also exhibited a value less than the lower limit value. Only upper limits are often determined in the literature, whereas lower limits were also determined in this study. For the obtained average values of diagnostic parameters, the limit values were found with a probability of 99.7%, which are deviations upward and downward from the mean-squared errors of the arithmetic means. The author's contribution was employed instead of the ± 3 standard deviations found in the literature, i.e., the $\pm 3\sigma_s$ (mean-squared error of the arithmetic mean) was used. The time waveforms of Figure 4 clearly show the pulses originating from fuel injection.

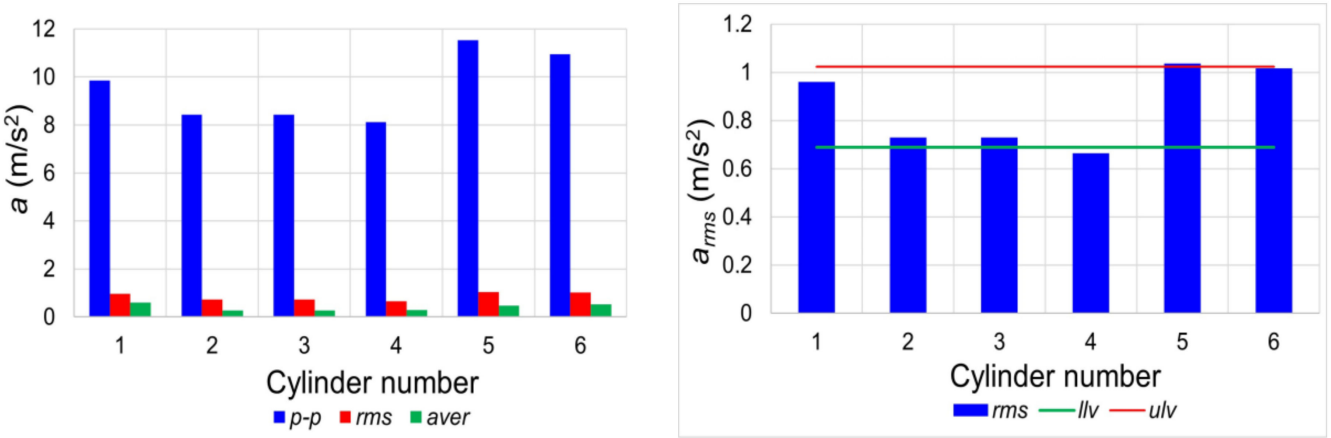

(**a**) (**b**)

Figure 5. Sample results of the analysis of vibration acceleration signals for cylinders No. 1–6 in the domain of amplitude (**a**) and root-mean-square (*rms*) values measured relative to the limit values (**b**): *p-p*—peak-to-peak value, *aver*—average value, *llv*—lower limit value and *ulv*—upper limit value.

The analysis of the signals in the amplitude domain demonstrated the usefulness of point amplitude estimates for detecting damage development.

3.3. Analysis in the Frequency Domain

To obtain reliable signal analysis results, it is advisable to conduct an analysis of the time domain and frequency domain, either separately or together. Figure 6a shows the spectra in Figure 4a for cylinder No. 1 in the suitability state, and before the damage in No. 5. Figure 6a shows that this is a polyharmonic and polyperiodic complex signal. Polyharmonic signals, in addition to the fundamental component at frequency f_p (usually rotational), contain superharmonic components at frequency if_p (i = 1, 2, 3, ... n) [3]. Polyharmonic signals consist of multiple polyharmonic signals with different fundamental frequencies [3].

The vibration acceleration spectra were divided into third-octave bands (Figure 6b), in which the powers of N_H harmonics, recorded in terms of mean and *rms* values, were determined in the octave (thirds) band of the spectrum according to the following relationship:

$$\widetilde{H}_{o,t} = \sqrt{N_H} = \left[\sum_{i=1}^{n} \frac{H_i^2}{2}\right]^{\frac{1}{2}} \tag{9}$$

where $\widetilde{H}_{o,t}$ is the partial *rms* value in the *i-th* octave (third) band, and H_i is the component of the amplitude spectrum.

Analyzing the frequency domain signals, damage-oriented symptoms were sought in octave and one-third octave bands (Figure 6). The measurement results in the frequency domain in the one-third octave bands are shown in Figure 6, in which, in (a), the average values of the amplitudes for cylinders No. 1 and No. 5 are presented. Figure 6b shows a

significant variation in some components' average amplitudes of the vibration acceleration signals (*aver*). Figure 6b displays the *rms* values of the amplitudes in the one-third octave bands for cylinders No. 1–6, along with the limit values (*llv* and *ulv*). Figure 6c shows that the upper limit value (*ulv*) for cylinder No. 5 exceeded that of the precritical damaged state.

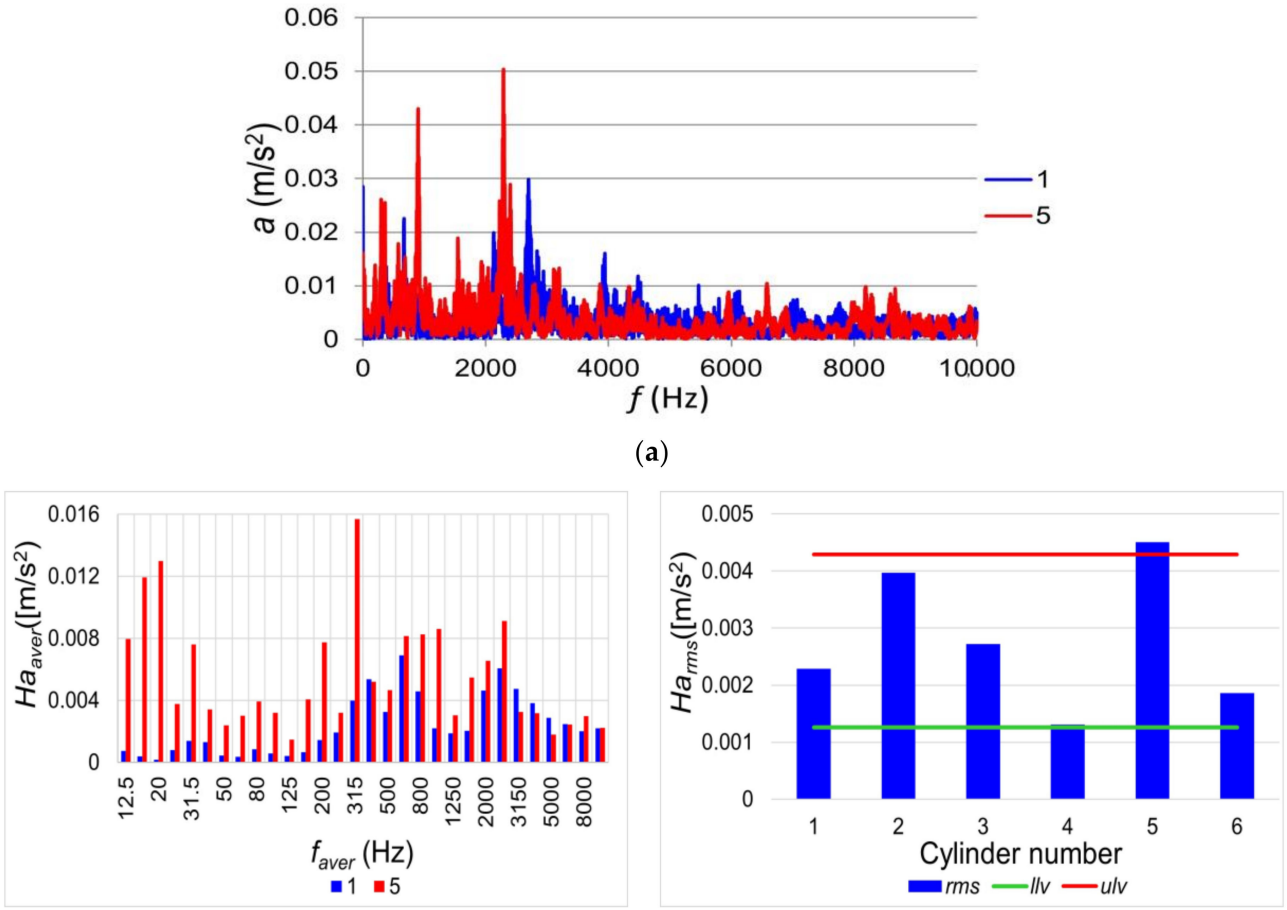

Figure 6. Amplitude-frequency spectrum (**a**), the average values of vibration acceleration amplitudes in one-third octave bands for cylinder No. 1 in suitability state and cylinder No. 5 before damage (**b**), and *rms* values of vibration acceleration amplitudes H_a in one-third octave bands for f_{aver} = 160 Hz with limit values (**c**): f_{aver}—center frequency, *llv*—lower limit value, and *ulv*—upper limit value.

After 247 h of test operation, the combustion engine was halted due to an increase in exhaust gas temperature to 600 °C at a 37.5% load. A breakage was found in the injector nozzle of cylinder No. 5 (Figure 7a). The cracking of the injector nozzle body resulted in intense fuel leakage, which is shown in Figure 7b for an exemplary nozzle in a suitable state (q_m = 0.0419 kg/s) and another nozzle with a cracked body (q_m = 0.1094 kg/s).

A large fuel leak occurred due to a broken-off section of the injector nozzle of cylinder No. 5, which diluted the lubricating oil with fuel. The oil analysis showed it was unsuitable for further operation due to its low flash point (165 °C) and reduced viscosity.

Repeated cyclic loading during operation under high pressure and thermal loads [15,20] tends to cause unexpected fatigue cracks. The lack of resistance, which led to failure, was observed using semiempirical growth formulas for defects that increased due to cyclic loading and caused severe damage. The data for injector nozzle cracking are presented in Table 2 to distinguish the phases of damage development in the marine engine's injector nozzles.

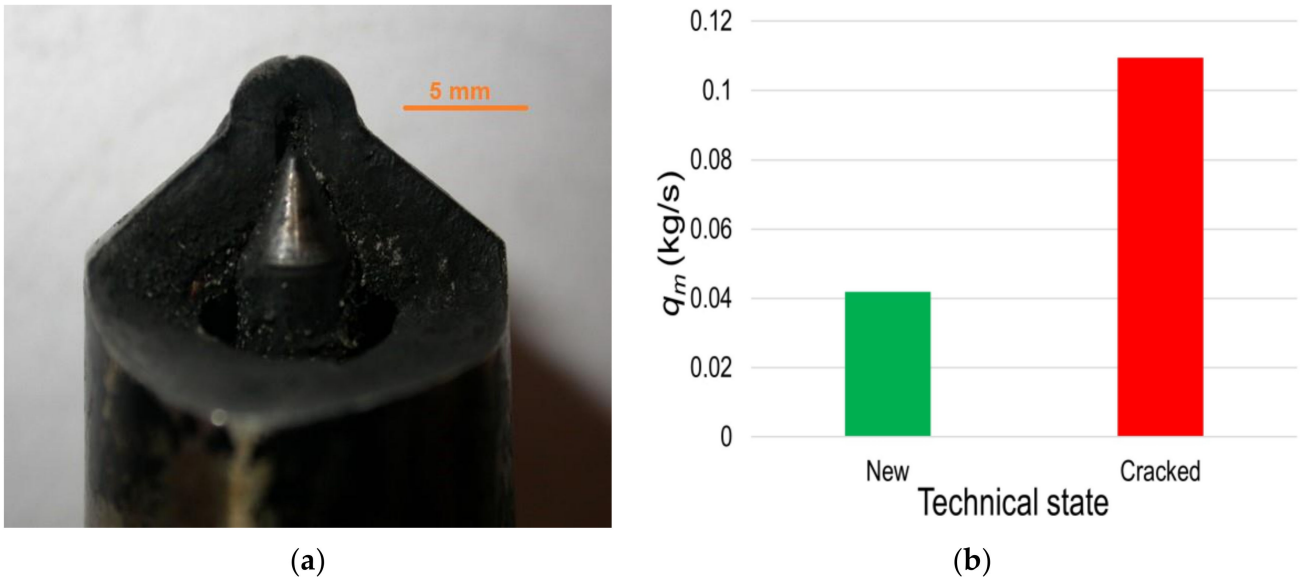

(**a**) (**b**)

Figure 7. Injector nozzle of the diagnosed 6AL20/24D engine with a broken part of the body (**a**) and mass flux q_m of the flowing fuel at the full needle lift for a nozzle in a suitable state and another nozzle with a cracked nozzle body (**b**).

Table 2. Phases of damage development leading to breakage of the injector nozzle body.

Phase Number	Description of the Crack Development Phase
1	Cracking
2	Crack propagation
3	A fragment tearing off
4	A fragment breaking off
5	Secondary damage to other objects

Analysis of the signals in the frequency domain also showed the existence of a large number of diagnostic symptoms related to damage development. Here, it is possible to compare the current and reference spectra without synchronization.

3.4. Wavelet Analysis

This study looked for suitable signal analysis methods, before using wavelet analysis. The analysis began with the Haar function. The basic Haar wavelet is defined as follows:

$$\Psi(\tau) = \begin{cases} 1 \text{ for } 0 \leq \tau \leq 0.5 \\ -1 \text{ for } 0.5 \leq \tau \leq 1 \\ 0 \text{ for } \tau < 0 \text{ and } \tau \geq 1 \end{cases} \quad (10)$$

The statistical measures of the output signal at different levels of approximation were determined. When using Haar wavelets at level 5 for the original signals (Figure 8a), for the mean and mode values, the highest sensitivity coefficient values were obtained for individual cylinders No. 1 to 6 from the available wavelet measures (Figure 8b). The maximum of the Haar wavelet (Figure 8c) was a more useful indicator for boundary values.

Figure 8 shows that the Harr wavelets resulted in the effective detection of the injector nozzle's propagating crack.

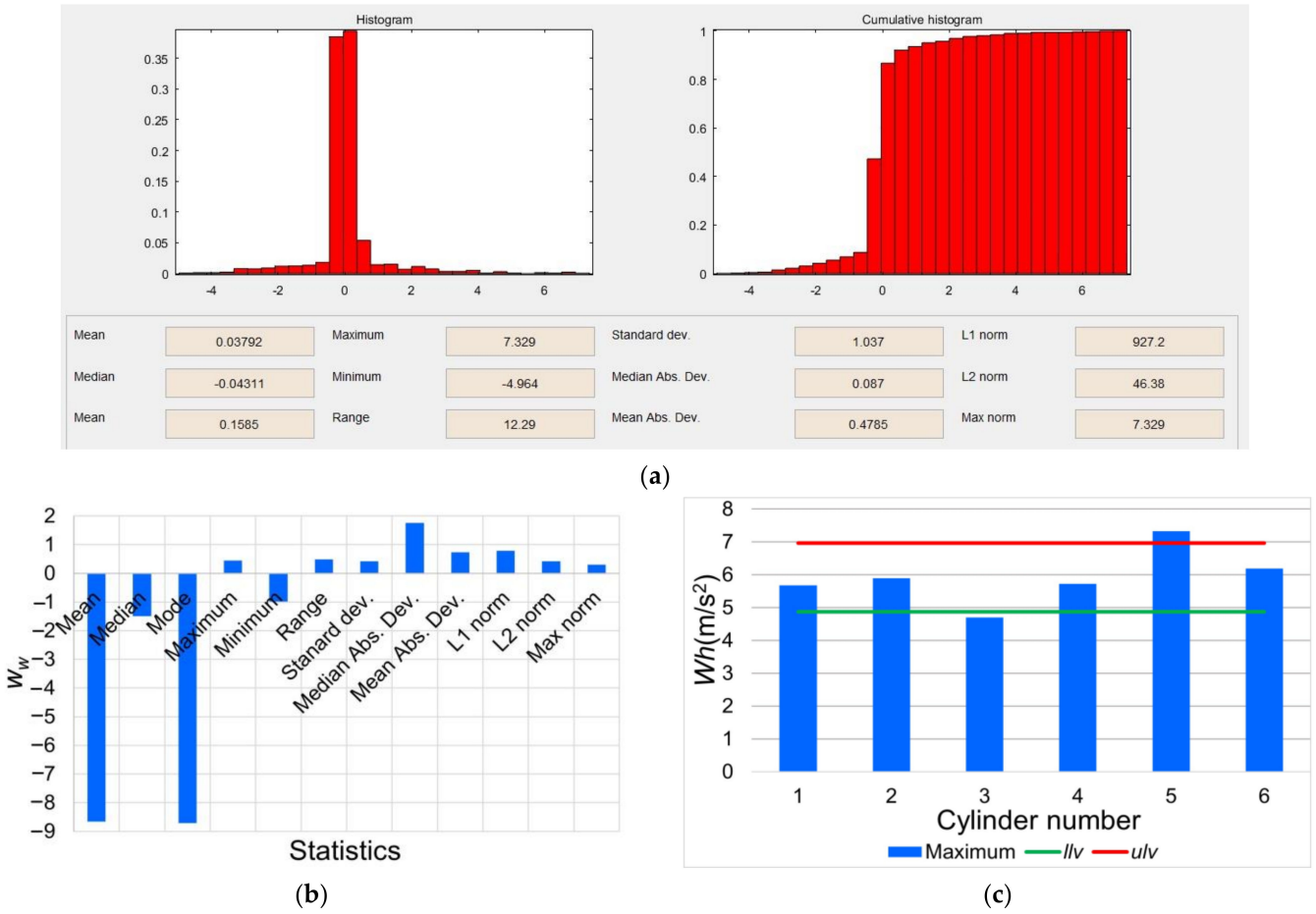

Figure 8. The results of the Haar wavelet statistics for the original vibration acceleration signal from cylinder No. 5 (**a**), the sensitivity results w_w of these statistics for individual cylinders (**b**), and more useful maximum values of the Haar wavelet W_h (**c**): *llv*—lower limit value; *ulv*—upper limit value.

3.5. Time-Frequency Analysis

Traditional frequency analysis is unsuitable for observing nonstationary signal properties with time-varying parameters. This is because an analysis using combined time-frequency representations of signals is required. These analyses can be divided into time-frequency and time-scalar analyses and interpreted as short-time spectral analyses [3].

Time-frequency analysis was performed to diagnose crack development, especially recommended for nonstationary and nonlinear signals, which can vary even within a single period of signal oscillation. In the engine under study, there were speed fluctuations. Figure 9a shows the time-frequency analysis for cylinder No. 1 in a suitable state, and Figure 9b shows the analysis for cylinder No. 5 with damage propagation.

There is little to be gleaned from the continuous wavelet transform and time–frequency analysis; therefore, image color analysis was used as an auxiliary procedure to evaluate them [34]. Thus, image analyses were used to process time-frequency diagrams similar to that for evaluating the wear of injector nozzles. In addition, studies were performed to calculate the global color measure for the suitability of cylinder No. 1 before the damage detection of nozzle No. 5. In this article, the global color measure of time-frequency analyses was determined from the contribution of the three primary colors according to the following relationship:

$$G_m = k_{eR}R \oplus k_{eG}G \oplus k_B B \tag{11}$$

where G_m is the global color measure of time-frequency, k_R is the weighting factor of red color R, k_G is the weighting factor of green color G, and k_B is the weighting factor of

blue color *B*. For these cases, the variation in color intensity and the values of the global color measure (1.02/1.00) was insignificant. Time-frequency analysis, other than effective visualization, has yet to prove useful.

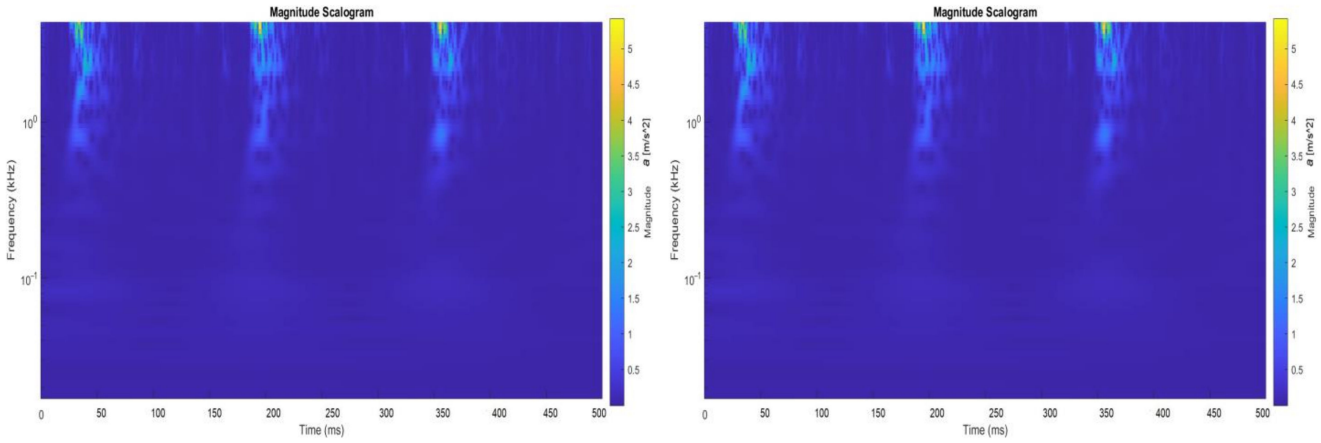

(**a**) (**b**)

Figure 9. The time-frequency analyses for cylinder No. 1 in a suitable state (**a**) and for cylinder No. 5 with damage propagation (**b**).

3.6. Application of Kurtosis

Crack propagation leads to random kinematic nodes and additional degrees of freedom, loss of function, and safety hazard. The following equation can describe the extent of fatigue development of the cracking of the nozzle nose:

$$D = C_1\left(1 - \frac{S(\tau)}{S(\tau_0)}\right) \tag{12}$$

where $C_1 = \frac{S(\tau)}{S(\tau) - S(\tau_f)}$ is used to determine the scaling factor, $S(\tau)$ is the diagnostic symptom for operation time τ, $S(\tau_0)$ is the diagnostic symptom for operation time τ_0, and $S(\tau_f)$ is the diagnostic symptom at the instant of nose breakage τ_f. The difference in the width of the energy-relevant band can be determined in the form of the spectral width factor to assess the damage development [6]:

$$\nu = \frac{m_2^2}{m_0 m_4} \tag{13}$$

where the spectral moments were calculated from the following formula:

$$m_k = \int_{-\infty}^{\infty} f^k S(f) df \tag{14}$$

where S is the measurement signal.

$$m_0 = \int_{-\infty}^{\infty} S(f) df \tag{15}$$

$$m_2 = \int_{-\infty}^{\infty} f^2 S(f) df \tag{16}$$

$$m_4 = \int_{-\infty}^{\infty} f^4 S(f) df \tag{17}$$

The kurtosis K is the fourth-degree moment equals:

$$K = \frac{\frac{1}{n}\sum_{i=1}^{n}\left(s_i - \bar{s}\right)^4}{\sigma^4} \quad (18)$$

where σ is the standard deviation.

Kurtosis measures the concentration of the results and determines how concentrated they are around the mean. Kurtosis was used because, according to Radkowski [6], kurtosis changes occur in the first low-energy phases of damage development. The values of kurtosis presented in the figure for individual cylinders of the tested engine did not indicate damage. For cylinder No. 5, the kurtosis values were between the limit values defining the suitability state, and for cylinder No. 1 was too low (Figure 10).

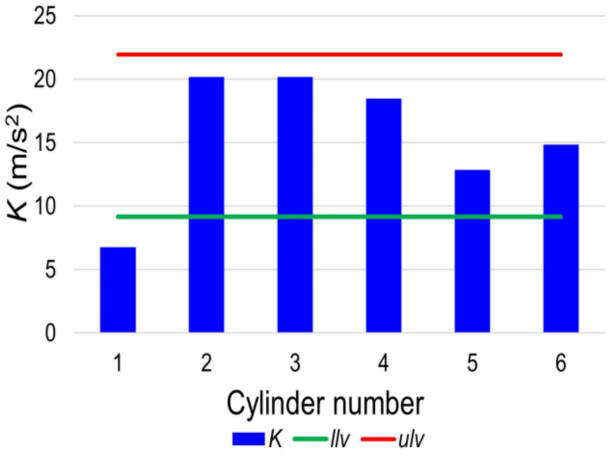

Figure 10. Kurtosis values K for individual cylinders of the tested engine with limit values: *llv*—lower limit value, *ulv*—upper limit value.

The kurtosis value in Figure 10 below the lower limit corresponds to the deregulation (reduction) in the injector opening pressure and lower value combustion pressure. This occurred for kurtosis, which is not the best diagnostic parameter.

3.7. Machine Learning Methods

Neural networks provide innovative solutions in the classification of technical states. In this work, a neural network was used to detect a developing crack in a marine internal combustion engine component.

This study aims to develop a neural network-based classification system for identifying signals in various technical states. The neural network was established considering the diagnostic parameters of the recorded signals in multiple domains, and predictive models capable of classifying unknown state symptoms were developed. A graphical diagram of the stages of the procedure, from the acquisition of signals from the internal combustion engine to the development of the classification and recognition model, is shown in Figure 11.

Classification is supervised, and semisupervised learning algorithms have been applied to binary problems. A semisupervised algorithm is a type of supervised machine learning in which the algorithm "learns" to classify new measurement data based on examples of selected data. The classification learner application was used to apply classification models interactively. Techniques such as machine learning and deep learning were employed, which enable machines to use the environment to improve tasks. In machine learning, a neural network classifier was chosen for all the neural networks.

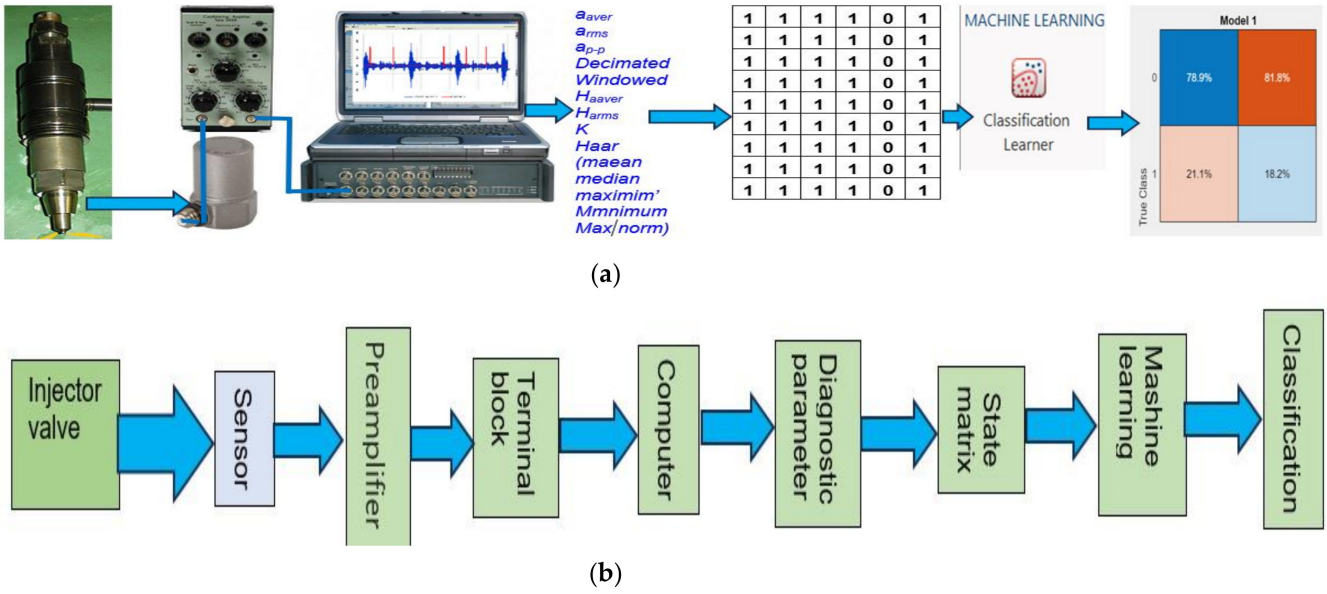

Figure 11. The architecture of the methodology from test object to state classification (**a**) and block diagram (**b**).

The classifier divides the feature space of a technical condition into decision areas in a part of the feature space such that all points located in the distinguished area correspond to the same class. The boundaries between these areas are called decision surfaces or decision boundaries. The following decision rules were used in this study:

- If $S(\tau_f) \geq llv$ and $S(\tau_f) \leq ulv$, then it indicates a suitable state;
- If $S(\tau_f) \leq llv$ and $S(\tau_f) \geq ulv$, then it indicates a state of unfitness.

The results from neural network classification depend on many factors, the most important of which is the quality of learning, testing, and validation. The error generated using a neural network depends on the weighting coefficients present in the network and can be refined using machine learning algorithms [35,36]. In practice, the learning coefficient determines the error correction amount and can change during the learning of the network, improving the quality of the results.

To evaluate the quality of learning, the GIGO (garbage in, garbage out) rule [37] was used to evaluate the quality of learning and learning data. Networks were evaluated using statistics as network quality coefficients for learning, testing, and validation sets [38].

The quality of the network was assessed in terms of its ability to generalize, and the measure was the quality of the validation sample, that is, the new data that had not been subjected to the learning process. In the classification model, "accuracy" was determined as the ratio of the number of correct predictions to the total number of predictions. These qualities can be expressed are Pearson correlation coefficients between the expected values and the network's prediction:

$$k = \frac{\sum_{i=1}^{n}\left(x_i - \bar{x}\right)\left(y_i - \bar{y}\right)}{\sqrt{\sum_{i=1}^{n}\left(x_i - \bar{x}\right)^2 \sum_{i=1}^{n}\left(y_i - \bar{y}\right)^2}} \tag{19}$$

where i is the consecutive number of the component of the diagnostic parameter, x_i is the consecutive value of the given input, $\bar{x}$ is the average value of the given input in the set of observations, and y_i is the consecutive value of the given diagnostic parameter.

These qualities are Pearson correlation coefficients between the expected values and the network's prediction, so a linear correlation of $\geq$70% in the learning set was considered a good result.

Many algorithms were tested in this research, some of which are presented. The classification learner tool of MATLAB 2022a achieved a validation accuracy of 85.1% for the support vector machine (SVM) neural networks and a testing accuracy above 80.9% for multiple models (Figure 12). A confounding matrix represents the number of observations and correctly classified data (blue diagonal), and the brown-colored diagonal represents the incorrectly classified data in percentages. This is the true-positive rate (*TPR*) matrix, which represents the percentage of correctly classified observations for correct class 1; false-negative rates (*FNR*) depict the percentage of incorrectly classified observations for incorrect class 0.

(**a**)

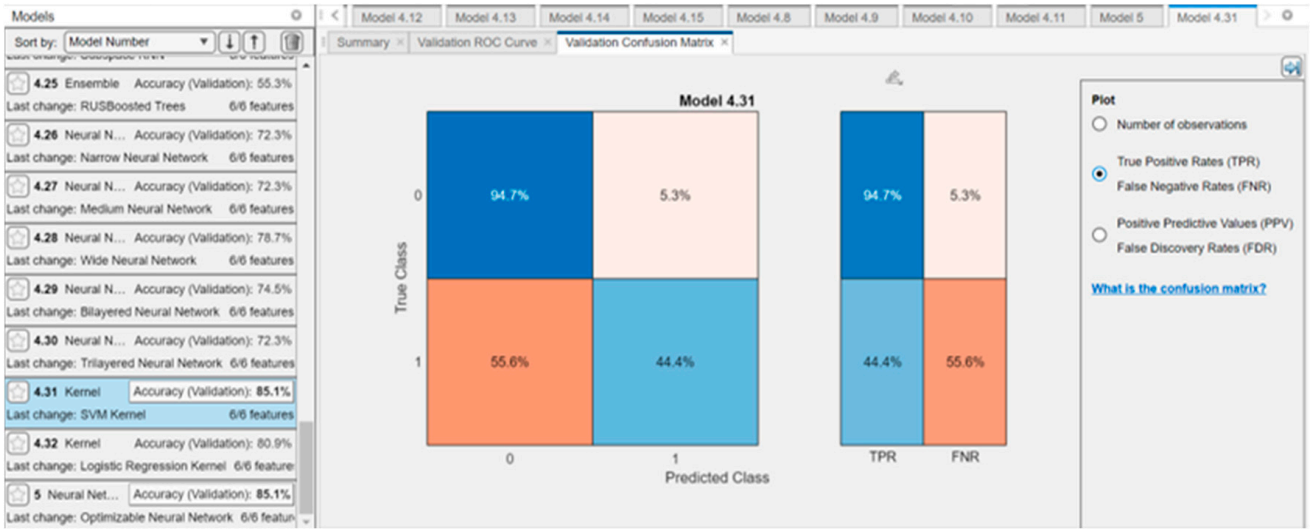

(**b**)

Figure 12. Test accuracy results for model 4.12 (**a**) and model 4.31 (**b**) classification of the used diagnostic parameters.

The quality of teaching, validation, and testing contributes to the accuracy of correct diagnosis in learning cases. The area under the curve (AUC) value measures the overall quality of the classifier. AUC values ranged from 0 to 1. Larger AUC values indicate better classifier performance. The closer the area under the curve (AUC) is to unity, the better the

model. The marker on the ROC plot shows the performance of the current classifier. The false-negative rate was calculated from the following relationship:

$$W_{FN} = \frac{FN}{TN + FN} \tag{20}$$

where FN is the number of false-negative classifications, and TN is the number of true-positive classifications.

The marker in Figure 13 displays the values of the false-positive rate and true-positive rate for the models 4.12 (a,b) and 4.31 (c,d) classifiers. For example, a true-positive rate of 0.74 indicates that the classifier correctly assigns 74% of the positive class observations to the positive class. As can be observed from the ROC and AUC values (Figure 11c,d), the results obtained using the network are satisfactory.

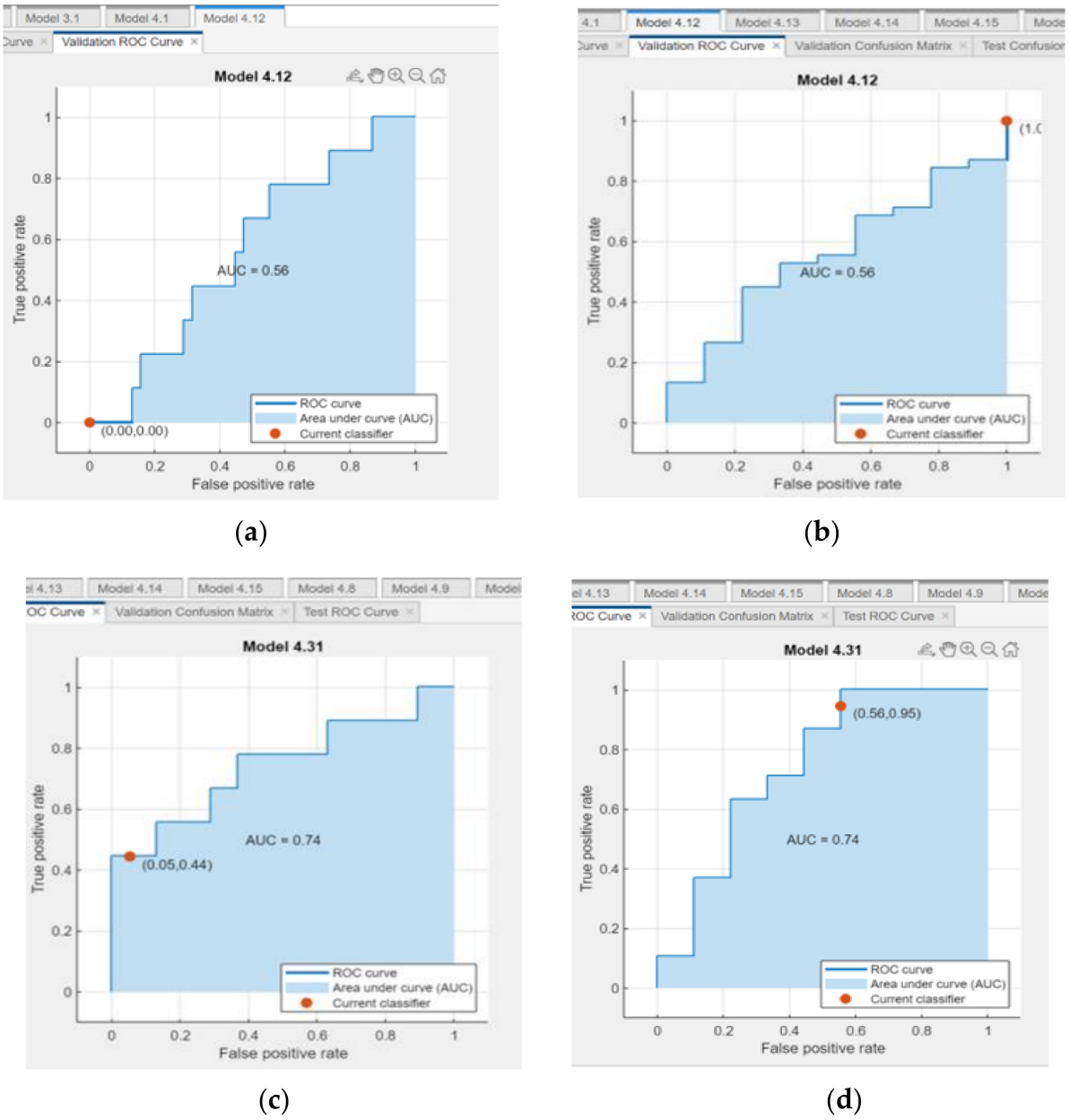

Figure 13. Test accuracy results for model 4.12 (**a**,**b**) and model 4.31 (**c**,**d**) classification of used diagnostic parameters for positive and negative classes.

The algorithm was also trained for hyperparameter optimization using the classification learner tool [39]. By default, this tool tunes parameters using Bayesian optimization. In the application of hyperparameter tuning, a point is a set of hyperparameter values, and the objective function is the loss function or classification error. Figure 14 shows the estimated minimum classification error. The dark blue point corresponds to the observed minimum classification errors calculated for a certain number of iterations using the optimization process.

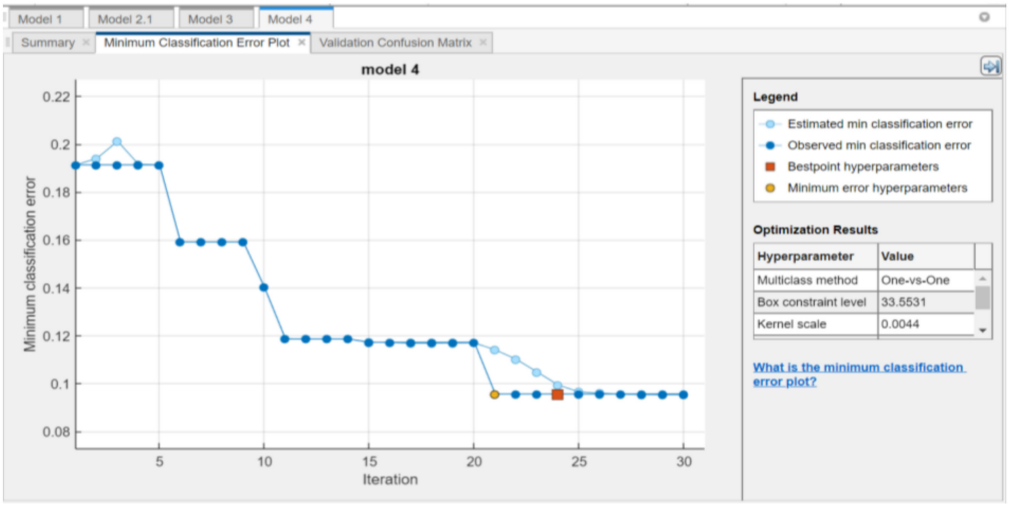

Figure 14. Minimum classification errors for 30 iterations of model 4.

In the Statistica program (Table 3), the testing quality was 80% for several networks, and the learning quality was 100% for the multilayer perceptron (MPL) 6-7-2 network. The values of the learning, testing, and validation quality, given (as a percentage) in Table 3, were close to ≥70%, and very close to ≥90% correlations were observed between the quantity of the diagnostic parameter values and the technical state classification values.

Table 3. Summary of active networks in the computer program Statistica.

Network ID	Network Name	Quality Learning	Quality of Testing	Quality of Validation
1	MLP 6-10-2	88.2353	80.00000	76.66667
2	MLP 6-5-2	88.2353	80.00000	76.66667
3	MLP 6-6-2	88.2353	80.00000	76.66667
4	MLP 6-6-2	94.1176	80.00000	76.66667
5	MLP 6-7-2	100.0000	80.00000	76.66667

Table 3 shows that the optimal network is MPL 6-7-2, comprising six input neurons, seven hidden layer neurons, and two neurons in the output layer. This network had the highest learning quality of 100% with the same quality of testing and validation.

The testing accuracy can be improved by discarding less sensitive diagnostic parameters and testing more networks. The obtained values of the diagnostic parameters were assigned binary numbers based on limit values to a suitable state (1) or a state of damage (0). The results obtained in MATLAB and Statistica computer programs are similar [38,40], which can be considered both satisfactory and encouraging for further research.

Studies in the literature have not determined the threshold of quality that can be considered suitable for classification; therefore, in this study, the strength of the relationship between variables in terms of the correlation coefficient values was considered the indicator of quality. Analyses were also performed to assess which artificial intelligence model was the most suitable for crack prediction.

3.8. Analysis of Obtained Results

The usefulness of the optimal diagnostic symptoms may be determined by the values of the correlation coefficient [9] between the individual cylinders and the sensitivity index (8) calculated for all cylinders separately, as well as the optimization performed considering the selected criteria. The sensitivity coefficient w_w was determined from the following relationship:

$$w_w = \frac{y_{imax} - y_{imin}}{\overline{y}} \tag{21}$$

where y_{imax} is the maximum value of the diagnostic parameter in the set of observations, y_{imin} is the minimum value of the diagnostic parameter in the collection of observations, and $\overline{y}$ is the average value of a diagnostic parameter in a group of observations.

The usefulness of the most diagnostically oriented symptoms was evaluated based on the determined correlation coefficient values and the sensitivity index between individual cylinders and for all cylinders separately (Figure 15).

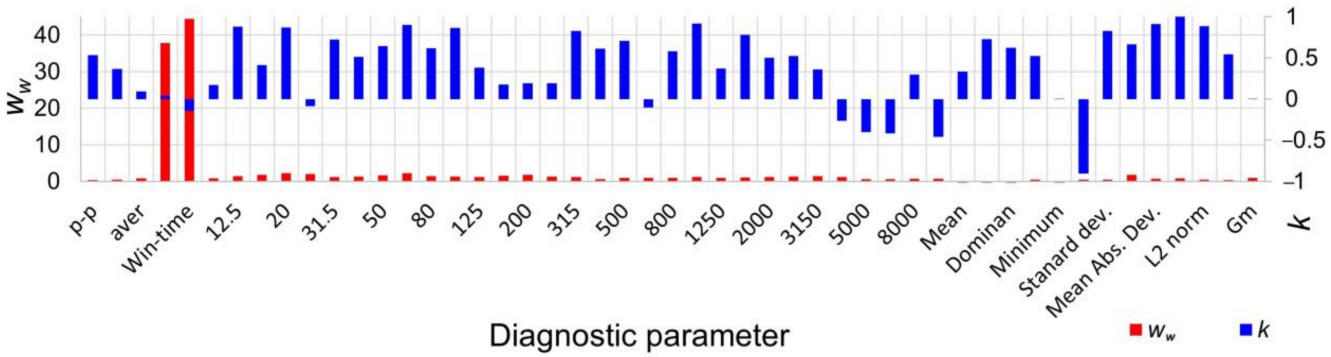

Figure 15. Assessment of the usefulness of diagnostic symptoms based on the correlation coefficient and sensitivity index value: k—correlation coefficient, w_w—sensitivity index.

The highest values of these coefficients were obtained for decimation, windowed time-domain, and Haar wavelet analyses.

Diagnostic tests can be optimized to select the most advantageous parameters for a given object and to determine the order of checks using the criteria [3]. Optimization was carried out in this work considering selected criteria such as the measurement sensor's location, signal analysis domain, correlation, and sensitivity of diagnostic symptom values with technical state features to minimize energy losses due to friction and, thus, reduce the fuel consumption of the diagnosed tribological pairs [9,29].

In terms of the output of vibration acceleration signals, the diagnostic parameter can be determined using the following formula:

$$a_p(\theta, \tau) = O[a_o(\theta, \tau)] = O[g_o(F, E_s, Z, Y), \tau] \tag{22}$$

where $a_p(\theta, \tau)$ is the parameter of vibration acceleration processes; τ is the dynamic time; θ is the time of operating element; F is the fuel feed vector, refrigerant feed, etc.; X is the vector of state features; E_s is the vector of control (fuel setting, engine load, and injection time); Z is the vector of disturbances; Y is the vector of output quantities; and O is the operator of the object performance.

The vector of vibration acceleration symptoms $S_a(r,\theta)$ is obtained during the monitoring of operation, whether the diagnostic parameters $a_p(\theta,\tau)$ are correlated (or uncorrelated) and sensitive to the characteristics of the technical states; whether they exceed the limit values is determined according to the following relationship:

$$S_{all} \leq S_a(r, \theta) = \Psi[r, X(\theta)] + Z(r, \theta) = A(w_w)[X(\theta)] + [Z(r, \theta)] \leq S_{aul} \tag{23}$$

where $A(w_w)$ is the sensitivity matrix of the linear expansion of the operator $\Psi[\cdot]$; $\Psi[\cdot]$ is the matrix operator of assignment; r is the distance resulting from the distribution of the propagated damage and the measurement sensor; S_{all} is the lower limit value of the diagnostic symptom; and S_{aul} is the upper limit value of the diagnostic symptom.

The model (24) allows for improving the current decisions on the state of the injector based on the experience gained, which is a combination of the results of signal analysis and diagnosed objects.

The experimental results show that the presented methods can accurately monitor fatigue crack growth. Industry 4.0 requires testing methods with advanced diagnostic and predictive algorithms to improve the accuracy of models. In addition, classification models were proposed to evaluate damage growth to enhance classification accuracy based on a machine learning matrix.

4. Discussion

The presented test results indicate that, in the operation of internal combustion engines, any initiated damage propagates during operation. This study presents original developments with little representation in the literature. Yet, modern methods of modeling compression ignition marine engine diagnostic solutions are needed. Therefore, developing real-time monitoring methods for fatigue crack initiation and propagation is crucial for the safe operation of transportation means.

It was revealed that the vibrations of combustion engines are closely associated with the technical state. Typically, more extensive wear or damage is associated with greater intensity of vibroacoustic phenomena and an increase in the impulse element of the signal. Experimental signals are typically complex and contain narrowband and broadband components. The problem is the selection of locations for measuring sensors, diagnostic parameters, and signal analysis domains. None of the cited publications have analyzed these factors in so many domains of signal analysis.

This type of research can be categorized as interdisciplinary research encompassing all stages of research, from the formulation of the research methods to the development of tools to support the implementation of these methods and the applications for modeling real mechanical systems.

The test results of the selected diagnostic parameters and the evaluation of their usefulness encourage further research. Future research directions concern the application of other signal parameters and parameters of working and accompanying processes. Limitations include the possibility of mounting sensors during operation, the difficulty of obtaining results from repetitive loads, the volume of data, etc.

5. Conclusions

Selected parameters of vibration signals for windowed time analysis, decimation, and some statistics of the Haar wavelet were determined to be damage-oriented with correlation coefficients close to 0.00 or 1.00 and sensitivity coefficients even above several hundred.

For the selection of diagnostic symptoms, the estimated limit values proved useful, which confirmed the differentiation between the technical states in various domains of the analysis of diagnostic signals. Symptoms of vibration acceleration in many research domains detected the developing damage 247 h before the failure.

Artificial neural networks with a test accuracy of 80% or higher were found to be suitable for identifying and classifying the technical state.

Comprehensive research on using multisymptom diagnostics to detect damage development enables the use of selected symptoms for applications in the operation of internal combustion engines. A particularly noteworthy contribution of this research is in determining the lower and upper limits that separate the different states of crack development of injector nozzles.

Funding: This research was conducted as a project financed by a subsidy of the Ministry of Education and Science for statutory activities 1/S/KE/23.

Institutional Review Board Statement: Not applicable.

Informed Consent Statement: Not applicable.

Data Availability Statement: Not applicable.

Acknowledgments: The author would like to thank the shipowner Polsteam for allowing the tests to be carried out on the vessel.

Conflicts of Interest: The author declares no conflict of interest.

References

1. Barczewski, R. *Diagnostic Oriented Methods of Short Time Processing of Vibroacoustic Signals*; Poznan University of Technology: Poznan, Poland, 2013; no. 504.
2. Piotrowski, J. *Measurements, Sensors and Measurement Methods of Selected Physical Quantities and Chemical Composition*; WNT: Warsaw, Poland, 2009.
3. Żółtowski, B.; Cempel, C. Elements of the theory of technical diagnostics. In *Engineering of Diagnostics Machines*; Society of Technical Diagnostics: Bydgoszcz, Poland, 2004; pp. 17–525.
4. Boguś, P. *Application of Nonlinear Methods of Signal Analysis in Combustion Engine Diagnostic*; Poznan University of Technology: Poznan, Poland, 2006; no. 398.
5. Dybala, J. *The Use of Vibroacoustic Signal in Technical Risk Analysis*; Institute for Sustainable Technologies: Radom, Poland, 2006.
6. Radkowski, S. *Vibroacoustic Diagnostics of Low-Energy Damage*; Institute for Sustainable Technologies: Warsaw/Radom, Poland, 2002.
7. Radkowski, S.; Jasiński, M. Diagnosis of the gigacycle fatigue processes in the gear. *Diagnostyka* **2005**, *36*, 13–23.
8. Miesowicz, K.; Staszewski, W.J.; Korbiel, T. Analysis of Barkhausen noise using wavelet-based fractal signal processing for fatigue crack detection. *Int. J. Fatigue* **2016**, *83*, 109–116. [CrossRef]
9. Monieta, J. Selection of Diagnostic Symptoms and Injection Subsystems of Marine Reciprocating Internal Combustion Engines. *Appl. Sci.* **2019**, *9*, 1540. [CrossRef]
10. Tomaszewski, F. *Problems of Determination of a Complex Mechanical Structure's Technical Condition Using Vibroacoustic Signal*; Habilitation Dissertation; Poznan University of Technology: Poznan, Poland, 1998; no. 337.
11. Czech, P.; Wojnar, G.; Warczek, J. Application of the discrete wavelet transform and probabilistic neural networks in IC engine fault diagnostics. *J. Vibroeng.* **2014**, *16*, 1619–1639.
12. Czech, P. Diagnosing a car engine fuel injectors' damage. Activities of Transport Telematics. Communications in Computer and Information Science 2013. In Proceedings of the 13th International Conference on Transport Systems Telematics (TST), Katowice, Poland, 23–26 October 2013; Volume 395, pp. 243–250.
13. Idzior, M.; Karpiuk, W. Investigations of the usefulness of dilatometric methods in the diagnostics of combustion engines. *Energies* **2021**, *14*, 6703. [CrossRef]
14. Ruddy, B.L.; Dowson, D.; Economus, P.N. A theoretical analysis of the twin land type of oil-control piston ring. *J. Mech. Eng. Sci.* **1981**, *23*, 51–62. [CrossRef]
15. Yu, Z.W.; Xu, X.L. Cracking damage of diesel engine injector nozzles. *Eng. Fail. Anal.* **2009**, *16*, 112–118. [CrossRef]
16. Xu, X.L.; Yu, Z.W. Cracking failure of locomotive diesel engine injector nozzles. *J. Fail. Anal. Prev.* **2015**, *15*, 513–520. [CrossRef]
17. Asi, O. Failure of a diesel engine injector nozzle by cavitation damage. *Eng. Fail. Anal.* **2006**, *13*, 1126–1133. [CrossRef]
18. Galle, J.; Verhelst, S.; Sierens, R.; Goyos, L.; Castaneda, R.; Verhaege, M.; Vervaeke, L.; Bastiaen, M. Failure of fuel injectors in a medium speed diesel engine operating on bio-oil. *Biomass Bioenergy* **2012**, *40*, 27–35. [CrossRef]
19. Madej, H.; Flekiewicz, M.; Sonar, G. Spatial-phase selection of diesel engine vibroacoustic signal for piston slap diagnostic. Jurna of KONES. *Powitani Transp.* **2007**, *2*, 133–144.
20. Namigtle-Jiménez, A.; Escobar-Jiménez, R.; Gómez-Aguilar, J.; García-Beltrán, C.; Téllez-Anguiano, A. Online ANN-based fault diagnosis implementation using an FPGA: Application in the EFI system of a vehicle. *ISA Trans.* **2019**, *100*, 358–372. [CrossRef] [PubMed]
21. Korczewski, Z. The conception of energetic investigations of the multisymptomatic fatigue of the simple mechanical system' constructional materials. *J. Pol. CIMAC* **2012**, *7*, 99–107.
22. Tabaszewski, M.; Szymanski, G.M. Engine valve clearance diagnostics based on vibration signals and machine learning methods. *Mainten. Reliab.* **2020**, *22*, 331–339. [CrossRef]
23. Zhao, H.; Mao, Z.; Chen, K.; Jiangn, Z. An intelligent fault diagnosis method for a diesel engine valve based on improved wavelet packet-Mel frequency and convolutional neural network. In Proceedings of the International Conference on Sensing, Diagnostics, Prognostics, and Control (SDPC), Beijing, China, 15–17 August 2019; pp. 354–359. [CrossRef]
24. Monieta, J.; Towiański, P. Investigations of undesirable events of anthropotechnical systems of marine power plants. *Sci. J. Marit. Univ. Szczec.* **2006**, *10*, 319–328.
25. Wang, R.H.; Chen, H.; Guan, C.A. Bayesian inference-based approach for performance prognostics towards uncertainty quantification and its applications on the marine diesel engine. *ISA Trans.* **2021**, *118*, 159–173. [CrossRef]

26. Niu, X.X.; Yang, C.L.; Wang, H.C.; Wang, Y.Y. Investigation of ANN and SVM based on limited samples for performance and emissions prediction of a CRDI-assisted marine diesel engine. *Appl. Therm. Eng.* **2017**, *111*, 1353–1364. [CrossRef]
27. Chybowski, L.; Bejger, A.; Gawdzińska, K. Application of subversion analysis in the search for the causes of cracking in a marine engine injector nozzle. *Int. J. Ind. Man. Eng.* **2018**, *12*, 302–308.
28. Nogin, S.; Semiao, J.; Monteiro, J. A Non-intrusive IoT System for the Detection of Faults in Internal Combustion Engines. In Proceedings of the 1st International Congress on Engineering and Sustainability in the XXI Century (INCREaSE), Faro, Portugal, 11–13 October 2017; pp. 338–358. [CrossRef]
29. Monieta, J.; Kasyk, L. Optimization of design and technology of injector nozzles in terms of minimizing energy losses on friction in compression ignition engines. *Appl. Sci.* **2021**, *11*, 7341. [CrossRef]
30. Monieta, J.; Nowicki, M. Experimental manners of an interference reduction of chosen measuring signals of a generating set in conditions of a marine power plants. *Diagnostyka* **2018**, *19*, 93–102. [CrossRef]
31. Monieta, J. Diagnostics of work process course in cylinders of marine reciprocating internal combustion engines using vibration signal. *Combust. Engines* **2013**, *3*, 153–160.
32. Monieta, J.; Sendecki, A. Database and knowledge about essential manufacturers of marine self-ignition engines. *J. Mar. Sci. Eng.* **2020**, *8*, 239. [CrossRef]
33. Monieta, J.; Łukomski, M. Methods and means of estimation of technical state features of the marine diesel engines injector nozzles type Sulzer 6AL20/24. *Sci. J. Marti. Univ. Szczecin* **2005**, *5*, 383–392.
34. Monieta, J.; Szmukała, M.; Adamczyk, F. The effect of natural deterioration on selected properties of rapeseed oil methyl esters. *Fuel* **2022**, *330*, 125606. [CrossRef]
35. Esposito, D.; Esposit, F. *Introducing Machine Learning*; Microsoft Press: Redmond, WA, USA, 2020; ISBN 978-0-13-556566-7.
36. Tadeusiewicz, R.; Szaleniec, M. *Lexicon of Neural Networks*; Publisher of the Project Science Foundation: Wrocław, Poland, 2015.
37. Papadokonstantakis, S.; Machefer, S.; Schnitzlein, K.; Lygeros, A.I. Variable selection and data pre-processing in NN modelling of complex chemical processes. *Comput. Chem. Eng.* **2005**, *29*, 1647–1659. [CrossRef]
38. Electronic Statistics Textbook. StatSoft 2011. Available online: https://www.statsoft.pl/textbook/stathome.html (accessed on 7 January 2023).
39. Patange, A.D.; Pardeshi, S.S.; Jegadeeshwaran, R.; Zarkar, A.; Verma, K. Augmentation of decision tree model through hyper-parameters tuning for monitoring of cutting tool faults based on vibration signatures. *J. Vib. Eng.* **2022**, 1–19. [CrossRef]
40. Jabłoński, A. *Condition Monitoring Algorithms in MATLAB*; Springer: Cham, Switzerland, 2021.